Combination of in vivo phage therapy data with in silico model highlights key parameters for pneumonia treatment efficacy

Raphaëlle Delattre, Jérémy Seurat, Feyrouz Haddad, Thu-Thuy Nguyen, Baptiste Gaborieau, Rokhaya Kane, Nicolas Dufour, Jean-Damien Ricard, Jérémie Guedj, Laurent Debarbieux

Cell Reports

Article

Combination of *in vivo* phage therapy data with *in silico* model highlights key parameters for pneumonia treatment efficacy

Graphical abstract

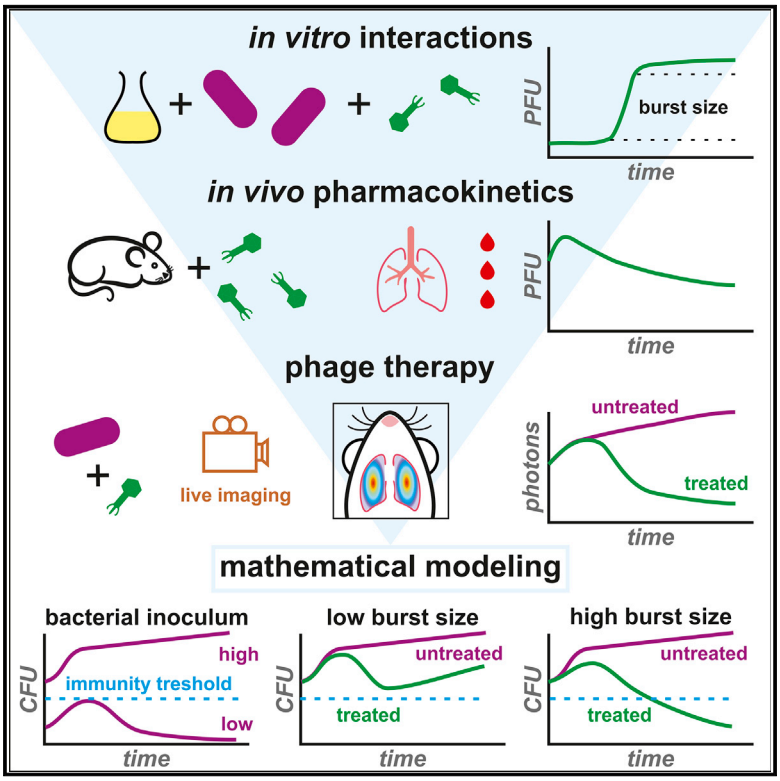

Authors

Raphaëlle Delattre, Jérémy Seurat, Feyrouz Haddad, ..., Jean-Damien Ricard, Jérémie Guedj, Laurent Debarbieux

Correspondence

jeremie.guedj@inserm.fr (J.G.), laurent.debarbieux@pasteur.fr (L.D.)

In brief

The clinical development of phage therapy to treat antibiotic-resistant bacterial infections requires understanding the dose-effect relationship. Delattre et al. use a murine pneumonia model to longitudinally record phage-bacteria interactions. Mathematical modeling characterizes the synergy between phages and the host immune response. Predictions of treatment outcome could guide clinicians.

Highlights

- Longitudinal records of pulmonary infections quantify the immunity threshold
- *In situ* amplification of phages is required for treatment efficacy
- A mathematical model predicts the outcome of phage-therapy treatment schemes

Delattre et al., 2022, Cell Reports *39*, 110825
May 17, 2022
https://doi.org/10.1016/j.celrep.2022.110825

CellPress

Cell Reports

CellPress
OPEN ACCESS

Article

Combination of *in vivo* phage therapy data with *in silico* model highlights key parameters for pneumonia treatment efficacy

Raphaëlle Delattre,[1,2,5] Jérémy Seurat,[2,5] Feyrouz Haddad,[1,2] Thu-Thuy Nguyen,[2] Baptiste Gaborieau,[1,2,3] Rokhaya Kane,[1] Nicolas Dufour,[4] Jean-Damien Ricard,[2,3] Jérémie Guedj,[2,6,*] and Laurent Debarbieux[1,6,7,*]

[1]Institut Pasteur, Université Paris Cité, CNRS UMR6047, Bacteriophage Bacterium Host, Paris 75015, France
[2]Université Paris Cité, INSERM U1137, IAME, Paris 75006, France
[3]APHP, Hôpital Louis Mourier, DMU ESPRIT, Service de Médecine Intensive Réanimation, Colombes, France
[4]Centre Hospitalier René Dubos, Médecine Intensive Réanimation, Cergy Pontoise 95503, France
[5]These authors contributed equally
[6]These authors contributed equally
[7]Lead contact
*Correspondence: jeremie.guedj@inserm.fr (J.G.), laurent.debarbieux@pasteur.fr (L.D.)
https://doi.org/10.1016/j.celrep.2022.110825

SUMMARY

The clinical (re)development of bacteriophage (phage) therapy to treat antibiotic-resistant infections faces the challenge of understanding the dynamics of phage-bacteria interactions in the *in vivo* context. Here, we develop a general strategy coupling *in vitro* and *in vivo* experiments with a mathematical model to characterize the interplay between phage and bacteria during pneumonia induced by a pathogenic strain of *Escherichia coli*. The model allows the estimation of several key parameters for phage therapeutic efficacy. In particular, it quantifies the impact of dose and route of phage administration as well as the synergism of phage and the innate immune response on bacterial clearance. Simulations predict a limited impact of the intrinsic phage characteristics in agreement with the current semi-empirical choices of phages for compassionate treatments. Model-based approaches will foster the deployment of future phage-therapy clinical trials.

INTRODUCTION

The pronounced slowdown in the discovery of new antibiotics to treat bacterial infections caused by multidrug resistant (MDR) pathogens has revived interest in bacteriophages (phages), viruses infecting bacteria (Gordillo Altamirano and Barr, 2019; Kortright et al., 2019). Pre-clinical experiments and several clinical case reports have demonstrated the potential of phages to successfully treat infections caused by MDR bacteria (Aslam et al., 2020; Bull et al., 2002; Corbellino et al., 2020; Jennes et al., 2017; Melo et al., 2020; Schooley et al., 2017). These successes are nonetheless balanced by unreported failures as well as disappointing clinical studies (Jault et al., 2019; Leitner et al., 2020; Sarker et al., 2016), showing that translation from experimental results to clinical trials remains challenging.

A major milestone for the widespread use in human populations is the determination of the optimal dose, route of administration, and treatment duration. This is a particularly complex endeavor for phages, as standard assessments of clinical pharmacology used to determine the processes of administration, distribution, metabolism, and excretion (ADME) of drugs are not adapted to phages. Indeed, phages massively replicate on their target bacteria, with kinetic parameters governing this viral amplification (receptor recognition, genome amplification, particles assembly, and bacterial lysis) being specific to each phage-bacteria pair (Dion et al., 2020). Furthermore, phages are naturally present in human-associated microbiotas, and their rate and route of elimination do not follow usual metabolic pathways of xenobiotic products through kidney or liver (Dabrowska and Abedon, 2019).

Here, we coupled *in vitro* and *in vivo* experiments with mathematical modeling to approach the key parameters of phage-bacteria-host interactions and guide treatment strategies. This approach has been successful in drug development for various chronic (HIV, hepatitis C virus and acute (Ebola, Zika, influenza) viral infections (Friberg and Guedj, 2020; Perelson and Guedj, 2015). Unlike previous models that focused on specific aspects of phage-bacteria, phage-host immune system, or bacteria-host immune system interactions (Cairns et al., 2009; Roach et al., 2017; Smith et al., 2011; Weld et al., 2004), here we aimed to design a synthetic, semi-mechanistic model that could be used to understand the tripartite phage-bacteria-host interactions *in vivo*. We designed specific experiments (Figure 1) to estimate the key parameters of phage-bacteria interactions using a previously characterized experimental model (Dufour et al., 2015). The virulent phage 536_P1 (141,471 bp), a *Myoviridae* belonging to the *Phapecoctavirus* genus, quickly (20 min) lyses the hypervirulent *Escherichia coli* strain 536 *in vitro*. Moreover, a single dose of phage 536_P1 administered intranasally to mice 2 h post-infection by a lethal dose of strain 536 rescued

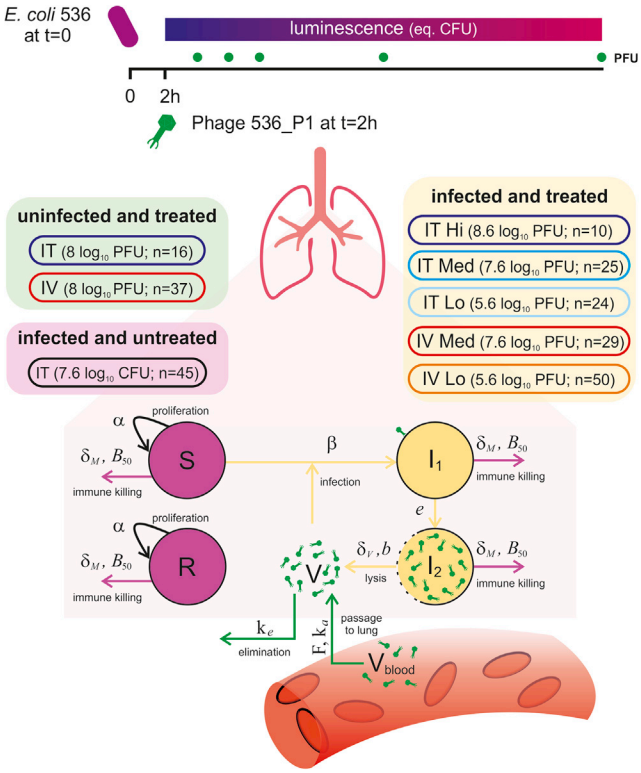

Figure 1. Schematic representation of the experimental design of the study

In vivo experiments were conducted in mice that were either (1) uninfected and treated (green box, with phages administered either intratracheally [IT] or intravenously [i.v.]), (2) infected and untreated (magenta box), or (3) infected and IT- or i.v.-treated at various doses (yellow box). The intensity of light emitted by *E. coli* strain 536-lux was recorded along all experiments and translated to bacterial lung density, while phage 536_P1 density was measured only once (upon sacrifice) in each animal at specific time points. A mathematical compartmental model was developed to fit to these data, with S, R, I_1, and I_2 representing the susceptible, refractory, infected non-productive, and productively infected bacteria, respectively, and V and V_{blood} the phage concentrations in lungs and blood, respectively. The arrows indicate the processes affecting each compartment. Model parameters characterizing these processes are indicated on these arrows, with α the bacterial growth rate, δ_M the maximal immunity effect, B_{50} the bacterial load leading to 50% of δ_M, β the infectivity rate, e the transition rate from latent to productive bacteria, δ_V the bacterial lysis rate, b the burst size, F the phage relative bioavailability in the lungs after i.v. compared with IT, k_a the phage absorption rate from the blood to the lungs and k_e the phage elimination rate in the lungs.

100% of animals, while untreated animals died within 72 h, demonstrating the efficacy of this phage to treat an acute pulmonary infection (Dufour et al., 2015).

Here, dynamic and direct microbiological data were collected from groups of animals that were either (bacterial) uninfected and (phage) treated, infected and untreated, or infected and treated, using different inoculum doses and routes of administration. These data led us to develop an original mathematical model recapitulating the tripartite interactions over time. This model identified key parameters affecting bacterial kinetics *in vivo*. It was then exploited to test scenarios including variations of phage intrinsic properties. The use of such a model will rationalize the phage choice, the dose, and the route of administration in order to optimize the efficacy of phage therapy.

RESULTS

Biodistribution of phage in uninfected mice

Our investigations started by assessing two routes of phage administration, intratracheal (IT) and intravenous (i.v.), in uninfected mice using a single dose of 8 $\log_{10}$ plaque-forming units (PFUs) of phage 536_P1 (Figure 2). The observed peak of median (interquartile range) phage concentrations in the lungs was reached 4 h post-administration by i.v. (5.1 [4.7, 5.5] $\log_{10}$ PFU/g) and was lower than the concentration observed post-administration by IT at the same time point (7.2 [6.8, 7.8] $\log_{10}$ PFU/g). The nearly 2-log difference showed that post-i.v. administration, only a fraction F of the phage, estimated to 0.02%, ultimately reached the lung compartment, leading to exposure approximately 5,000 times lower than post IT administration, and an estimation of the absorption rate into the lung compartment, k_a, of 0.3 h^{-1} (Equations 1 and 2). During the 48 h post-phage administration, the kinetics of the phage elimination rate in the lungs was slow following IT administration with an estimated half-life value of 12 h ($\log(2)/k_e(IT)$), while it was much faster following i.v. administration, with an estimated value of 3 h (Table 1).

Bacterial kinetics in infected, untreated mice

IT administration of the *E. coli* strain 536 led to a large variability in the lung bacterial load of untreated animals (N = 45), as measured by emitted luminescence and colony-forming unit (CFU)eq/g (see STAR Methods and Figure S1). Two h post-infection, bacterial load ranged between 5.0 and 9.9 $\log_{10}$ CFUeq/g (Figure 3), allowing us to evaluate the impact of phage across the large spectrum of values that can be observed in clinical conditions (Jiang et al., 2014). The large range of effective inoculums also informed on the threshold of bacterial density, above which the immune response of the host cannot control the infection. When the bacterial load was greater than 6.8 $\log_{10}$ CFUeq/g at 2 h post-infection, the bacterial density increased continuously and led to rapid death of all animals within 72 h. In contrast, below this threshold, a reduction of the bacterial density was generally observed, likely reflecting the effect of the immune response in clearing the infection (Figures 3 and S2).

Bacterial and phage kinetics in infected, treated mice

Next, using the same infection procedure as above, mice (N = 138) were treated 2 h post-infection with various doses of phage 536_P1 (low dose: 5.6, medium dose: 6.6, high dose: 7.6 $\log_{10}$ PFU), administered either by IT or i.v. route. The initial effective median bacterial inoculum in the lungs 2 h post-infection was similar across treatment groups, with levels of 6.9 (6.1, 8.0), 7.2 (6.3, 8.5), and 6.7 (6.3, 7.8) $\log_{10}$ CFUeq/g in untreated and IT- and i.v.-treated animals, respectively (Figure 3).

Globally, phage density in the lungs of IT- and i.v.-treated animals reached values 2- to 3-$\log_{10}$ higher than in uninfected animals, showing that phages rapidly encountered bacteria and efficiently replicated (Figure 2). At 4 h post-phage administration (6 h post-bacterial infection), the median titer of phage in the

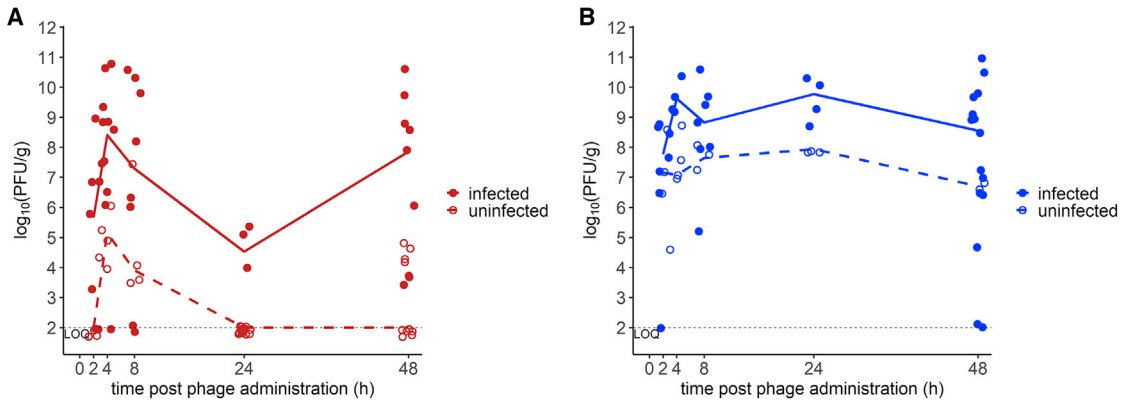

Figure 2. Distribution of phage 536_P1 in lungs following two routes of administration

(A and B) Lungs of uninfected (empty circles, N = 53) and *E. coli*-infected (filled circles, N = 76) mice were homogenized at 2, 4, 8, 24, or 48 h post-administration of a single dose of phage 536_P1 (8 $\log_{10}$ PFU in uninfected mice and 5.6, 7.6, or 8.6 $\log_{10}$ PFU in infected mice), either by i.v. (A, red) or IT (B, blue) route. Lines connect the median phage concentrations at each time point (dashed lines, uninfected; full lines, infected). The black dotted line represents the limit of quantification (LOQ = 2 $\log_{10}$ PFU/g).

lungs of IT-treated mice (N = 59) was 9.6 [9.3, 9.9] $\log_{10}$ PFU/g as compared with 7.1 [7.1, 7.4] $\log_{10}$ PFU/g in uninfected, i.t.-treated mice (N = 16). A similar difference was also observed in i.v.-treated animals (N = 79), with phage concentrations of 8.4 (7.0, 9.1) $\log_{10}$ PFU/g as compared with 5.1 (4.7, 5.5) $\log_{10}$ PFU/g in uninfected, i.v.-treated animals (N = 37) (Figure 2).

To illustrate the impact of the above phage amplification on disease progression, bacterial kinetics and survival were reported following the stratification of animals by the bacterial load measured 2 h post-infection (Figure 4). Phage therapy had no significant effect on bacterial kinetics and survival in animals having a low bacterial load (<6.8 $\log_{10}$ CFUeq/g, N = 78), reflecting the effective role of the immune response to clear the pathogen. By contrast, in animals having a higher load ($\geq$6.8 $\log_{10}$ CFUeq/g, N = 99), treated animals showed a faster kinetics of the bacterial control (p = 0.028).

Unraveling bacteria-phage interaction using a mathematical model

Next, we used the data from both infected and uninfected animals together with parameters determined *in vitro* (see STAR Methods) to build a mathematical model of phage-bacteria-host interaction (Equations 4, 5, 6, 7, 8, 9, and 10; Data S1; Figure 1).

Fitting the model to bacterial load data, we first determined that a model accounting for the control of bacterial growth by the innate immune response was needed to recapitulate the threshold effect associated with the effective bacterial inoculum. This phenomenon could be well captured using our model (Equation 3), with estimates of δ_M, the maximal decay induced by the immune response, of 6.8 $\log_{10}$ CFUeq/g/h and B_{50}, the bacterial load needed to reach $\delta_M/2$, of 7.4 $\log_{10}$ CFUeq/g. This corresponds to a threshold for bacterial control equal to 6.94 $\log_{10}$ CFUeq/g. Thus, if the administered bacterial inoculum, B_0, was below this value, bacteria were rapidly eliminated by the immune system with a rate of δ_M/B_{50} = 0.3 h^{-1}, corresponding to a half-life of 2.3 h. However, when the bacterial inoculum was above this value, the model predicts a saturation of the immune response, enabling bacterial growth with a bacterium doubling time estimated at 3.5 h.

In vitro experiments allowed us to estimate two key parameters of phage dynamics that could not be identified *in vivo*, namely the median eclipse phase and the burst size (see STAR Methods and Figure S3). Assuming that these parameters had the same value *in vivo*, we could then estimate the *in vivo* infection rate of bacteria by phages, denoted as β, to -6.9 $\log_{10}$ g/CFU/h and the *in vivo* elimination rate of phage-infected bacteria, δ_V, to 0.09 h^{-1} (e.g., a half-life of 7.7 h), which is slower than *in vitro* estimation (1.39 h^{-1}).

Finally, we also used the model to assess the impact of bacterial kinetics on survival. Assuming a log-linear effect of bacterial load on the instantaneous risk of death, *h(t)*, the bacterial load was found to be highly associated with death (γ = 1.44, p < 10^{-3}, Wald test). This corresponds to a hazard ratio of 4.2; in other words, an increase of 2 log of the bacterial load raised the instantaneous risk of death by ~18. The joint model developed could simultaneously recapitulate bacterial kinetics, phage counts, and survival rate (Figures 5, S4, and S5), despite the heterogeneity of the individual profiles experimentally observed (Figures 5 and S2).

Effects of phage dose and route of administration on the bacterial kinetics

The model was then used to identify the key factors governing bacterial kinetics. Unsurprisingly, the bacterial inoculum, B_0, was the most important parameter. In animals with B_0 <6 $\log_{10}$ CFUeq/g, bacterial loads rapidly decreased below the limit of quantification within 48 h regardless of treatment. In animals with large bacterial inoculum B_0 >8 $\log_{10}$ CFUeq/g, phage therapy was not sufficient to control the continuous growth of bacteria regardless of the route and administered phage dose (Figure 6). The benefit of phage therapy was apparent mostly for animals having an intermediate effective inoculum size, e.g., 6 < B_0 < 8 $\log_{10}$ CFUeq/g. In those animals, the larger ratio of

Table 1. Parameter estimates of the phage-bacteria dynamics model

Parameter	Name	Unit	Fixed/estimated from	Fixed effect (rse, %)	SD of random effect (rse, %)
Bacterial growth rate	α	h^{-1}	untreated infected	0.21 (–)	0 (–)
Initial number of bacteria	B_0	log $_{10}$CFU g^{-1}	untreated infected	7.1 (1)	0.14 (6)
Bacterial-load plateau	B_{max}	log $_{10}$CFU g^{-1}	untreated infected	10.4 (–)	0 (–)
Time for immunity activation	t_I	h	untreated infected	3.0 (–)	0 (–)
Maximal immunity effect	δ_M	CFU g^{-1} h^{-1}	untreated infected	6.7 10^6 (–)	0.05 (–)
Bacterial load for 50% of δ_M	B_{50}	CFU g^{-1}	untreated infected	2.3 10^7 (–)	0 (–)
Infectivity rate	β	log_{10} g CFU^{-1} h^{-1}	treated infected	-6.9 (7)	0.11 (43)
Transition rate	e	h^{-1}	*in vitro*	1.2 (–)	0 (–)
Lysis rate	δ_V	h^{-1}	treated infected	0.09 (25)	0 (–)
Burst size	b	PFU CFU^{-1}	*in vitro*	570 (–)	0 (–)
Relative bioavailability (i.v./IT)	F	–	treated uninfected	0.0002 (–)	0 (–)
Phage absorption rate	k_a	h^{-1}	treated uninfected	0.3 (–)	0 (–)
Phage elimination rate after IT	$k_e(IT)$	h^{-1}	treated uninfected	0.058 (–)	0 (–)
Phage elimination rate after i.v.	$k_e(IV)$	h^{-1}	treated uninfected	0.23 (–)	0 (–)
Phage distribution weight	W	g	treated uninfected	1 (–)	0 (–)
Initial refractory proportion	f	–	treated infected	0.105 (45)	2.8 (19)
Weibull shape	κ	–	treated infected	1.8 (11)	0 (–)
Weibull scale	λ	h^{-1}	treated infected	2.4 10^4 (98)	0 (–)
Impact of bacterial kinetics on death	γ	g CFU^{-1}	treated infected	1.44 (13)	0 (–)
Additive error on bacterial load	σ_B	log $_{10}$CFU g^{-1}	treated infected	–	0.47 (4)
Additive error on phage concentration	σ_V	log $_{10}$PFU g^{-1}	treated infected	–	2.6 (11)

SD, standard deviation; rse, relative standard error.

phage to bacteria led to a large number of bacteria being rapidly infected by phages, which prevented bacterial growth and maintained the bacterial load under control by the immune response. Bacterial-load decline was biphasic, with a rapid decline in the first 4 h of treatment, mainly due to the decay of susceptible bacteria (S) by phages, followed by a slower decline afterward. This slower second phase was attributed in our model to the unrestricted replication of a sub-population of bacteria that were not eliminated by phages (V), representing both phage-resistant and -inaccessible (spatially out of reach) bacteria (R).

The initial proportion of the phage-refractory population was estimated to be 10% (Table 1) but could be variable across individuals (from 0.03% to 76%). The dynamics of refractory bacteria was individual dependent, leading to either a slow but continuous bacterial decline or a rebound of fully refractory bacteria within 24–48 h (see individual examples in Figure 5). Importantly, the need to incorporate a compartment of refractory bacteria in the model was strongly supported by the data and led to a significant improvement of the data fitting ($p < 10^{-3}$, likelihood ratio test, data not shown).

The raw data did not allow us to observe a role of the route of administration in the treatment outcome, except with a low bacterial inoculum (B_0 = 6 log_{10} CFUeq/g) for which the rapid clearance of bacteria limited the encounter rate with phage. With this inoculum, relative to the kinetics in the untreated group, simulations indicated that an IT or i.v. medium dose of phages halved the total bacterial load in 3.1 and 8.1 h after administration, respectively. Our simulations also indicated that IT and i.v. treatments otherwise led to similarly high phages concentrations (>7 log_{10} PFU/g) in lungs (Figure 6). IT administration was, however, associated with a substantially faster time to peak viral load, and this difference was particularly apparent with a low or intermediate bacterial inoculum. For instance, with an intermediate bacterial inoculum (B_0 =7 log_{10} CFUeq/g), the time to peak viral load varied between 1.6 (IT high dose) and 6.0 h (i.v. IV low dose). As a consequence of this delay in phage maximal replication, the i.v. route had a lower efficiency to stop bacterial growth, with a time to peak bacterial load that could be as long as 4.0 h (i.v. low dose), to less than 1.1 h with the IT route (IT low dose), and as low as 0.3 h in the case of the IT high dose. Overall, with this lethal intermediate inoculum, the bacteria grew exponentially in untreated mice, whereas the bacterial load declined in all phage-treated groups. Therefore, in any phage-treated group, the median total bacterial load was increasingly lower than that of the untreated group. For instance, 24 h after administration, the bacterial load in treated groups was more than 100 times lower than in the untreated group (Figure 6).

Effects of phage characteristics on the bacterial kinetics

Finally, we also used the model to explore the effect of intrinsic phage characteristics, namely burst size and lysis

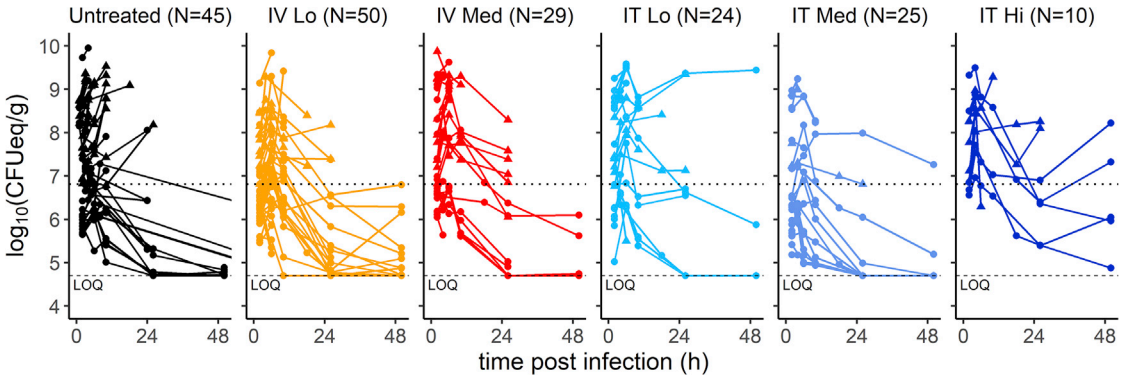

Figure 3. Kinetics of bacterial densities in untreated and phage-treated animals

CFU equivalent data from bioluminescent recordings of infected animals, which were either untreated (black) or treated with phage 536_P1 administered by i.v. (low dose = 5.6 $\log_{10}$ PFU, yellow, or medium dose = 7.6 $\log_{10}$ PFU, red) or IT (low dose, cyan, medium dose, blue, or high dose = 8.6 $\log_{10}$ PFU, dark blue). The dotted horizontal line at 6.8 $\log_{10}$ CFUeq/g corresponds to the threshold value of bacterial load at 2 h post-infection, below which all animals controlled the infection. The dashed line represents the LOQ of bacterial load (LOQ = 4.7 $\log_{10}$ CFUeq/g).

rate, on the bacterial kinetics. A 10-fold reduction in burst size (i.e., 57 PFU/CFU) predicted a larger impact of the route of administration, with a time to bacterial peak of 10 h post-i.v. compared with less than 3 h post-IT administration. Even when using a low dose of phage, the time to bacterial peak relative to untreated bacterial load was estimated at 12 h post-IT compared with 20 h post-i.v. (Figure S6). However, a higher lysis rate value counter-balanced the effects of a low burst-size value (Figure S7), showing the sensitivity of the model to phage characteristics.

DISCUSSION

Despite many encouraging data from both ancient literature and recent compassionate treatments, phage therapy remains underexploited, notably because of ambiguous results from clinical trials (Luong et al., 2020). In fact, the translation from *in vitro* to clinical conditions remains unmet, in particular since using phages as a drug requires specific methods to elaborate a rational scheme for safe and optimal administration. While some studies performed *in silico* or in laboratory conditions (Cairns et al., 2009; Kasman et al., 2002; Leung and Weitz, 2017; Payne and Jansen, 2001, 2003) led to the proposal of several mathematical models of phage-bacteria interactions, very few studies conducted *in vivo* incorporated the immune response (Dabrowska and Abedon, 2019; Roach et al., 2017).

Our experimental approach was inspired from work performed during the development of new drugs, where longitudinal pharmacokinetic and pharmacodynamic data are collected to understand the exposure-response relationship and optimize the dosing regimen (Marshall et al., 2019). It is important to acknowledge that bioluminescence is nonetheless a proxy of bacterial load compared with CFU counts from lung samples, as reflected by the measurement error associated with bioluminescent data (parameter σ_B; Table 1). However, this limitation is largely compensated by longitudinal recordings that provide a unique insight on the determinants of bacterial kinetics for each animal.

The acute murine lung infection induced by bacterial pathogens that we used for this study imposed two constraints. First, less than 1-log variation of the bacterial inoculum can lead to contrasted outputs from rapid (24 h) mortality to no lethality (B.G., L.D., and G. Nouailles-Kursar unpublished observations with various strains of *E. coli* or *Pseudomonas aeruginosa* for which preliminary experiments were performed to identify the most appropriate bacterial inoculum). Second, the high pathogenicity of pathogens necessitated a phage administration 2 h post-infection to preserve a high survival rate of treated animals (Debarbieux et al., 2010). It is worth noting that until the early 2000s, *Enterobacteriaceae* were not considered major pathogens responsible for ventilator-associated pneumonia (VAP) (Chastre and Fagon, 2002). However, recent data have consistently shown that *Enterobacteriaceae* are now frequent etiologic agents of VAP, more frequently encountered than *Pseudomonas aeruginosa* and *Staphylococcus aureus* (Fihman et al., 2015; Hamet et al., 2012; Kollef et al., 2017). In particular, several studies have clearly identified specific traits of strains of *E. coli* responsible for intensive care unit (ICU)-acquired pneumonia (La Combe et al., 2019; Messika et al., 2012).

The heterogeneity of the initial bacterial loads observed 2 h post-infection provided a large range of situations reflecting clinical situations (Jiang et al., 2014). The variety of individual profiles was captured by using non-linear mixed-effect models to estimate phage-bacterial interaction, a statistical approach that borrows strength from the between-subjects variability to increase the precision of parameter estimation, and tease out the effects of bacteria parameters, doses, and routes of administration. A direct consequence of the above conditions was the precise quantification of the threshold value (6.94 $\log_{10}$ CFUeq/g), above which the immune response was overwhelmed in the absence of phage therapy.

The modeling of phage-bacteria interactions in the host also unraveled less-evident factors, such as the role of a refractory bacterial population to capture bacterial-load kinetics. This compartment could not be phenotypically characterized but encompasses bacteria that are escaping phage predation because

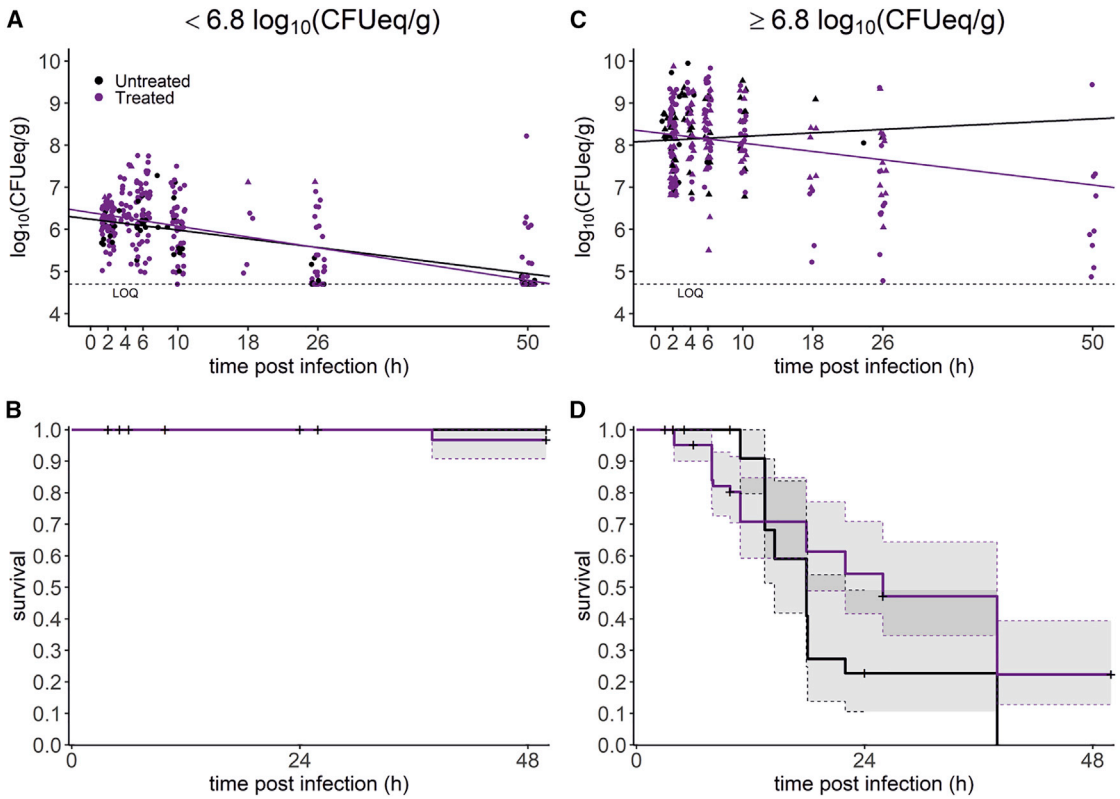

Figure 4. Bacterial load and survival of infected animals stratified by the pulmonary bacterial load at 2 h post-infection

Infected animals were untreated (black) or phage treated (purple). (A–D) The left panels (A and B) show animals with a low bacterial load (N = 78: 15 untreated, 63 treated), while the right panels (C and D) show animals with a high bacterial load (N = 99: 28 untreated, 71 treated). Of note, 6 animals sacrificed at 2 h post infection were not considered here. The top panels (A and C) show bacterial loads over time, with circles corresponding to live animals and triangles to animals that died before the scheduled sacrifice time. The difference between untreated and treated groups was assessed using a linear mixed-effects model, where the slope of bacterial change over time was adjusted on both the bacterial load value and the presence of treatment. The effect of treatment on bacterial kinetics was significant ($p = 0.028$, likelihood ratio test). Solid lines represent the median bacterial load predictions obtained with this model. The bottom panels (B and D) represent survival curves, with crosses indicating sacrifice time. The difference between untreated and treated groups was assessed using a log-rank tests (B, $p = 0.53$; D, $p = 0.08$).

they are phage resistant and/or they remain spatially inaccessible to phages (Leung and Weitz, 2017; Lourenco et al., 2020; Sousa and Rocha, 2019). The inclusion of this compartment is supported by both the emergence of phage resistance observed *in vitro* after 10 h of incubation with phage 536_P1 (Figure S4) and by previous studies showing that the spatial distribution of bacteria in organs makes some of them inaccessible to phages (Lourenco et al., 2020; Sousa and Rocha, 2019). This was also in agreement with the modelling of phage therapy in immunocompromised hosts (Roach et al., 2017). Despite the large variation of the bacterial loads that directly affect the initial density of this refractory population, our model could appropriately recapitulate the kinetics of phage-bacteria interactions for each individual mouse, including the survival probability, testifying to its robustness. In addition, simulations performed with larger or lower burst sizes and lysis rates showed that the model predicts outputs that are in agreement with results from animal studies in which different phages were used to treat bacterial infections (Alemayehu et al., 2012; Carmody et al., 2010; Henry et al., 2013; Morello et al., 2011).

To ensure that the model recapitulates kinetics of phage-bacteria interactions during therapy, it was necessary to use, as much as possible, parameters deduced from animal experiments instead of *in vitro* conditions. For instance, the growth rate of bacteria, infectivity rate, and lysis rate were all deduced from experimental data. Nevertheless, some parameters should be more deeply investigated to improve the fidelity of the model. For instance, growth of the refractory population was approximated as similar to the susceptible bacteria, neglecting the possibility that the fitness of mutants might be affected in the host. Indeed, such mutants could be, either or both, less virulent and strongly affected in their growth, allowing immune cells to eliminate them more effectively (Oechslin et al., 2017; Pouillot et al., 2012; Smith et al., 1987). The involvement of the immune response in the success of respiratory phage therapy was previously demonstrated and modeled but remains mechanistically poorly explored (Roach et al., 2017). In this work, we chose to account for the immune response in a synthetic way that encompasses mechanical factors, such as mucins and surfactant proteins, as well as various cellular actors of the innate immune system (Bergeron et al., 1998; Levin et al.,

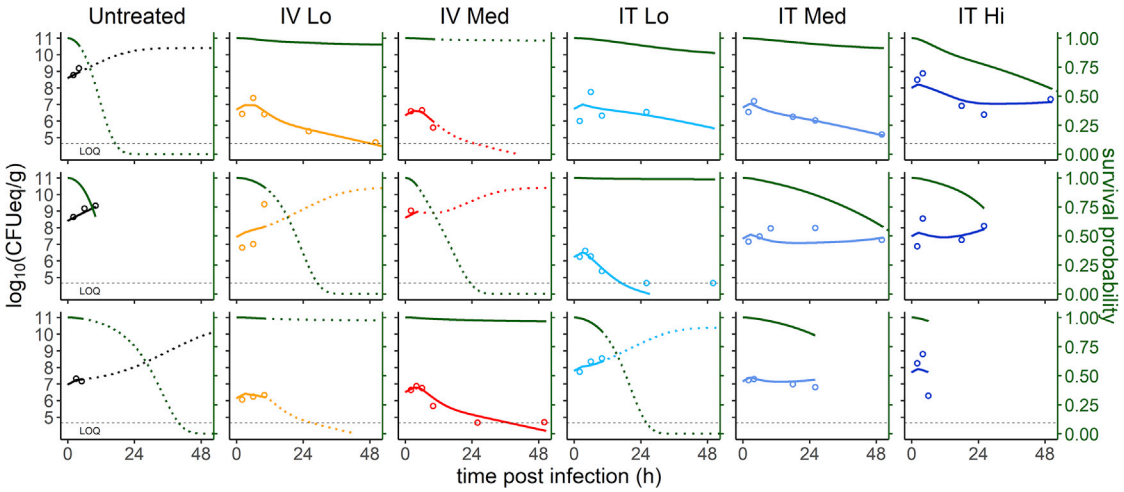

Figure 5. The mathematical model recapitulates the individual variations of the pulmonary bacterial loads and estimates the survival of infected animals

Data and model predictions for three mice (lines) randomly chosen from each experimental group (columns) are shown. The circles correspond to the pulmonary bacterial loads, the color lines correspond to the individual predictions from the model, and the green line represents the predicted survival probability. Lines are solid between t = 0 and the last observation time point (death or pre-specified sacrifice) and are dotted after the pre-specified sacrifice. Interrupted lines indicate the death of animals before the pre-specified time point. The horizontal dashed line represents the LOQ (LOQ = 4.7 $\log_{10}$ CFUeq/g).

2017; Marriott and Dockrell, 2007). However, the immune response would have been more mechanistically characterized if several markers (cytokines, immune cells) had been monitored. Our model also considers the lung compartment homogeneous, which ignores the complex structure of this organ that will most likely affect phage-bacteria interactions.

Predictions from the mathematical model showed the importance of viral load, burst size, and lysis rate to fully capture bacterial kinetics and animal outcomes. Therefore, for a suboptimal couple phage bacteria, which may often take place in clinics, the administration route, and to a lesser degree, the dose, will play a role in the rate at which bacterial growth will be controlled. This supports the determination of key parameters of phage-bacteria interactions, such as the infectivity rate and the lysis rate, for optimizing the phage-administration scheme. However, when the dose and route of administration are appropriately chosen, the model predicted that substantial variations of the intrinsic characteristics of phages (burst size and lysis rate) were not jeopardizing the treatment outcome, which fits with the current semi-empirical choice of phages for compassionate treatments. Indeed, currently, phages are chosen exclusively for their capacity to infect bacteria on *in vitro* conditions where phage-bacteria interactions are artificially optimized. To further evaluate the model, we performed simulations (external visual predictive check) from previous data obtained several years apart with the same phage-bacteria couple (Dufour et al., 2015). Despite a different route of administration (intranasal) for both the bacteria and the phage, we found that the model predicted acceptable results compared with the *in vivo* data, which argues in favor of its robustness and its putative relevance for many other phages (Figure S8).

Limitations of the study

The use of bioluminescent data as a proxy for CFU counts is limited by the accuracy of the correlation curve, which may be improved by lowering the delay between recording the photon emission from the animals and the actual plating of samples in selective media. In the model, we compensated this limitation by taking into account the error measurements (parameter σB). Another limitation is a lack of the phenotypic characterization of bacteria of the refractory compartment. The initial dispersion of phages in the lungs will not be sufficient to reach every single bacterial cell, but it remains unknown whether their amplification over time will be high enough and, at the same time, how it would influence the selection of phage-resistant bacteria. The susceptibility to phages of bacteria recovered from lung tissues collected should inform on the rate at which phage-resistant bacteria grow over time.

To conclude, the model developed during this work could be used to predict the efficacy of virtually any phage for which a minimum set of *in vitro* and *in vivo* data must be obtained, which will considerably lower the number of experiments needed to validate such a phage during pre-clinical development. Beyond phage therapy, the model could also be implemented to test combined anti-infectious therapies such as the association of phages with antibiotics (Lin et al., 2020).

STAR★METHODS

Detailed methods are provided in the online version of this paper and include the following:

- KEY RESOURCES TABLE
- RESOURCE AVAILABILITY
  - Lead contact
  - Materials availability
  - Data and code availability
- EXPERIMENTAL MODELS AND SUBJECT DETAILS
  - Ethic statement
  - Phages and bacterial strains

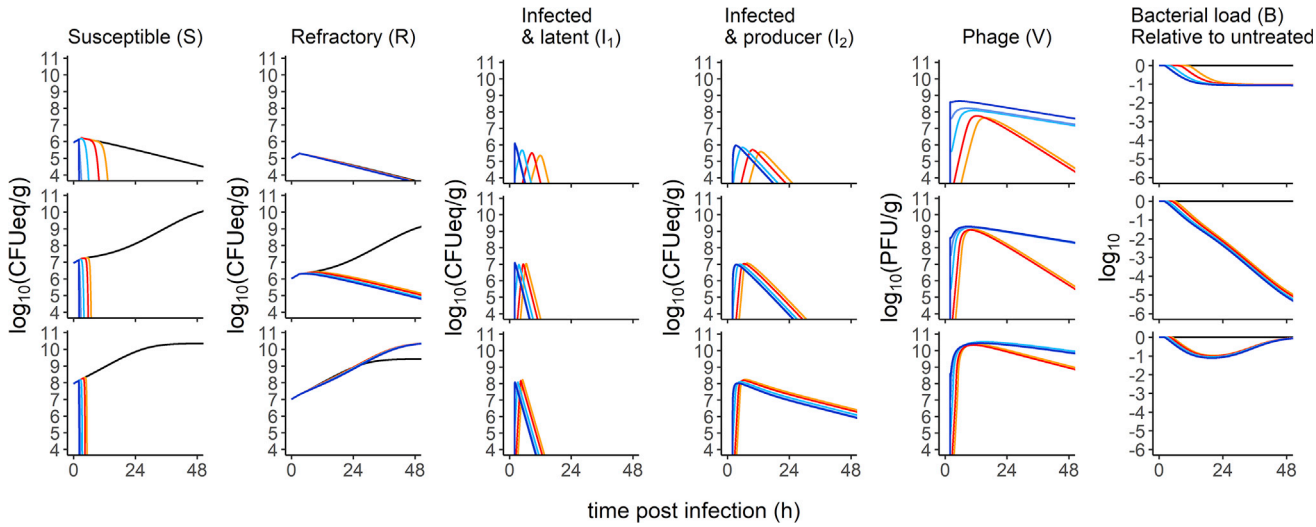

Figure 6. Simulations of different bacterial inoculums inform on the impact of refractory bacteria

Median profile assuming initial bacterial inoculums of 6, 7, and 8 $\log_{10}$ CFUeq/g (top, middle, and bottom lines, respectively). Predictions were calculated for each bacterial population (S, R, I_1, and I_2) and phages (V). The last column represents the ratio of the total bacterial load ($B = S + R + I_1 + I_2$) in the treated groups to that of the untreated group. The colors are indicative of both the route and the dose of phage administered: untreated (black), i.v.-Lo (5.6 $\log_{10}$ PFU, orange), i.v.-Med (7.6 $\log_{10}$ PFU, red), IT-Lo (cyan), IT-med (blue), and IT-high (8.6 $\log_{10}$ PFU, dark blue).

SUPPLEMENTAL INFORMATION

Supplemental information can be found online at https://doi.org/10.1016/j.celrep.2022.110825.

ACKNOWLEDGMENTS

This work was partly funded by ANSM (Agence Nationale de Sécurité du Médicament et des Produits de Santé) project no. HAP-2019-S003. B.G. received support from AIHP (Amicale des Anciens Internes des Hôpitaux de Paris). R.D. and N.D. both received, independently, support from Poste d'Accueil APHP/IP. We thank Hervé Le Nagard and Lionel de la Tribouille for the use of the CATIBioMed calculus facility.

AUTHOR CONTRIBUTIONS

J.-D.R., J.G., L.D., and R.D. conceived the study and secured funding. B.G., F.H., R.D., and R.K. performed experiments. J.-D.R., J.G., J.S., L.D., and R.D. analyzed the data. J.G., J.S., and T.-T.N. performed modeling. N.D. provided feedback. J.S. and R.D. wrote the first draft. J.G. and L.D. reviewed and edited final draft.

DECLARATION OF INTERESTS

The authors declare no competing interests.

Received: April 8, 2021
Revised: October 19, 2021
Accepted: April 25, 2022
Published: May 17, 2022

REFERENCES

Alemayehu, D., Casey, P.G., McAuliffe, O., Guinane, C.M., Martin, J.G., Shanahan, F., Coffey, A., Ross, R.P., and Hill, C. (2012). Bacteriophages φMR299-2 and φNH-4 can eliminate Pseudomonas aeruginosa in the murine lung and on cystic fibrosis lung airway cells. mBio *3*, e00029–00012. https://doi.org/10.1128/mBio.00029-12.

Aslam, S., Lampley, E., Wooten, D., Karris, M., Benson, C., Strathdee, S., and Schooley, R.T. (2020). Lessons learned from the first 10 consecutive cases of intravenous bacteriophage therapy to treat multidrug-resistant bacterial infections at a single center in the United States. Open Forum Infect. Dis. *7*, ofaa389. https://doi.org/10.1093/ofid/ofaa389.

Bergeron, Y., Ouellet, N., Deslauriers, A.M., Simard, M., Olivier, M., and Bergeron, M.G. (1998). Cytokine kinetics and other host factors in response to pneumococcal pulmonary infection in mice. Infect. Immun. *66*, 912–922. https://doi.org/10.1128/iai.66.3.912-922.1998.

Bergstrand, M., Hooker, A.C., Wallin, J.E., and Karlsson, M.O. (2011). Prediction-corrected visual predictive checks for diagnosing nonlinear mixed-effects models. AAPS J. *13*, 143–151. https://doi.org/10.1208/s12248-011-9255-z.

Brzuszkiewicz, E., Bruggemann, H., Liesegang, H., Emmerth, M., Olschlager, T., Nagy, G., Albermann, K., Wagner, C., Buchrieser, C., Emody, L., et al. (2006). How to become a uropathogen: comparative genomic analysis of extraintestinal pathogenic Escherichia coli strains. Proc. Natl. Acad. Sci. U S A *103*, 12879–12884. https://doi.org/10.1073/pnas.0603038103.

Bull, J.J., Levin, B.R., DeRouin, T., Walker, N., and Bloch, C.A. (2002). Dynamics of success and failure in phage and antibiotic therapy in experimental infections. BMC Microbiol. *2*, 35. https://doi.org/10.1186/1471-2180-2-35.

Cairns, B.J., Timms, A.R., Jansen, V.A.A., Connerton, I.F., and Payne, R.J.H. (2009). Quantitative models of in vitro bacteriophage-host dynamics and their application to phage therapy. PLoS Pathog. *5*, e1000253. https://doi.org/10.1371/journal.ppat.1000253.

Carmody, L.A., Gill, J.J., Summer, E.J., Sajjan, U.S., Gonzalez, C.F., Young, R.F., and LiPuma, J.J. (2010). Efficacy of bacteriophage therapy in a model of Burkholderia cenocepacia pulmonary infection. J. Infect. Dis. *201*, 264–271. https://doi.org/10.1086/649227.

Chastre, J., and Fagon, J.Y. (2002). Ventilator-associated pneumonia. Am. J. Respir. Crit. Care Med. *165*, 867–903. https://doi.org/10.1164/ajrccm.165.7.2105078.

Corbellino, M., Kieffer, N., Kutateladze, M., Balarjishvili, N., Leshkasheli, L., Askilashvili, L., Tsertsvadze, G., Rimoldi, S.G., Nizharadze, D., Hoyle, N., et al. (2020). Eradication of a multidrug-resistant, carbapenemase-producing Klebsiella pneumoniae isolate following oral and intra-rectal therapy with a custom made, lytic bacteriophage preparation. Clin. Infect. Dis. *70*, 1998–2001. https://doi.org/10.1093/cid/ciz782.

Dabrowska, K., and Abedon, S.T. (2019). Pharmacologically aware phage therapy: pharmacodynamic and pharmacokinetic obstacles to phage antibacterial action in animal and human bodies. Microbiol. Mol. Biol. Rev. *83*, e00012-19. https://doi.org/10.1128/mmbr.00012-19.

Debarbieux, L., Leduc, D., Maura, D., Morello, E., Criscuolo, A., Grossi, O., Balloy, V., and Touqui, L. (2010). Bacteriophages can treat and prevent Pseudomonas aeruginosa lung infections. J. Infect. Dis. *201*, 1096–1104. https://doi.org/10.1086/651135.

Desmee, S., Mentre, F., Veyrat-Follet, C., and Guedj, J. (2015). Nonlinear mixed-effect models for prostate-specific antigen kinetics and link with survival in the context of metastatic prostate cancer: a comparison by simulation of two-stage and joint approaches. AAPS J. *17*, 691–699. https://doi.org/10.1208/s12248-015-9745-5.

Dion, M.B., Oechslin, F., and Moineau, S. (2020). Phage diversity, genomics and phylogeny. Nat. Rev. Microbiol. *18*, 125–138. https://doi.org/10.1038/s41579-019-0311-5.

Dufour, N., Debarbieux, L., Fromentin, M., and Ricard, J.D. (2015). Treatment of highly virulent extraintestinal pathogenic Escherichia coli pneumonia with bacteriophages. Crit. Care Med. *43*, e190–198. https://doi.org/10.1097/ccm.0000000000000968.

Dufour, N., Delattre, R., Chevallereau, A., Ricard, J.D., and Debarbieux, L. (2019). Phage therapy of pneumonia is not associated with an overstimulation of the inflammatory response compared to antibiotic treatment in mice. Antimicrob. Agents Chemother. *63*, e00379-19. https://doi.org/10.1128/aac.00379-19.

Fihman, V., Messika, J., Hajage, D., Tournier, V., Gaudry, S., Magdoud, F., Barnaud, G., Billard-Pomares, T., Branger, C., Dreyfuss, D., and Ricard, J.D. (2015). Five-year trends for ventilator-associated pneumonia: correlation between microbiological findings and antimicrobial drug consumption. Int. J. Antimicrob. Agents *46*, 518–525. https://doi.org/10.1016/j.ijantimicag.2015.07.010.

Friberg, L.E., and Guedj, J. (2020). Acute bacterial or viral infection-What's the difference? A perspective from PKPD modellers. Clin. Microbiol. Infect. *26*, 1133–1136. https://doi.org/10.1016/j.cmi.2019.12.008.

Gordillo Altamirano, F.L., and Barr, J.J. (2019). Phage therapy in the postantibiotic era. Clin. Microbiol. Rev. *32*, e00066-18. https://doi.org/10.1128/cmr.00066-18.

Hamet, M., Pavon, A., Dalle, F., Pechinot, A., Prin, S., Quenot, J.P., and Charles, P.E. (2012). Candida spp. airway colonization could promote antibiotic-resistant bacteria selection in patients with suspected ventilator-associated pneumonia. Intensive Care Med. *38*, 1272–1279. https://doi.org/10.1007/s00134-012-2584-2.

Henry, M., Lavigne, R., and Debarbieux, L. (2013). Predicting in vivo efficacy of therapeutic bacteriophages used to treat pulmonary infections. Antimicrob. Agents Chemother. *57*, 5961–5968. https://doi.org/10.1128/aac.01596-13.

Hyman, P., and Abedon, S.T. (2009). Practical methods for determining phage growth parameters. Methods Mol. Biol. *501*, 175–202. https://doi.org/10.1007/978-1-60327-164-6_18.

Jault, P., Leclerc, T., Jennes, S., Pirnay, J.P., Que, Y.A., Resch, G., Rousseau, A.F., Ravat, F., Carsin, H., Le Floch, R., et al. (2019). Efficacy and tolerability of a cocktail of bacteriophages to treat burn wounds infected by Pseudomonas aeruginosa (PhagoBurn): a randomised, controlled, double-blind phase 1/2 trial. Lancet Infect. Dis. *19*, 35–45. https://doi.org/10.1016/s1473-3099(18)30482-1.

Jennes, S., Merabishvili, M., Soentjens, P., Pang, K.W., Rose, T., Keersebilck, E., Soete, O., Francois, P.M., Teodorescu, S., Verween, G., et al. (2017). Use of bacteriophages in the treatment of colistin-only-sensitive Pseudomonas aeruginosa septicaemia in a patient with acute kidney injury-a case report. Crit. Care *21*, 129. https://doi.org/10.1186/s13054-017-1709-y.

Jiang, W., Yan, Y., Ji, W., Wang, Y., and Chen, Z. (2014). Clinical significance of different bacterial load of Mycoplasma pneumoniae in patients with Mycoplasma pneumoniae pneumonia. Braz. J. Infect. Dis. *18*, 124–128. https://doi.org/10.1016/j.bjid.2013.06.004.

Kasman, L.M., Kasman, A., Westwater, C., Dolan, J., Schmidt, M.G., and Norris, J.S. (2002). Overcoming the phage replication threshold: a mathematical model with implications for phage therapy. J. Virol. *76*, 5557–5564. https://doi.org/10.1128/jvi.76.11.5557-5564.2002.

Kollef, M.H., Ricard, J.D., Roux, D., Francois, B., Ischaki, E., Rozgonyi, Z., Boulain, T., Ivanyi, Z., Janos, G., Garot, D., et al. (2017). A randomized trial of the amikacin fosfomycin inhalation system for the adjunctive therapy of Gram-Negative ventilator-associated pneumonia: IASIS trial. Chest *151*, 1239–1246. https://doi.org/10.1016/j.chest.2016.11.026.

Kortright, K.E., Chan, B.K., Koff, J.L., and Turner, P.E. (2019). Phage therapy: a renewed approach to combat antibiotic-resistant bacteria. Cell Host Microbe *25*, 219–232. https://doi.org/10.1016/j.chom.2019.01.014.

Kuhn, E., and Lavielle, M. (2005). Maximum likelihood estimation in nonlinear mixed effects models. Comput. Stat. Data Anal. *49*, 1020–1038. https://doi.org/10.1016/j.csda.2004.07.002.

La Combe, B., Clermont, O., Messika, J., Eveillard, M., Kouatchet, A., Lasocki, S., Corvec, S., Lakhal, K., Billard-Pomares, T., Fernandes, R., et al. (2019). Pneumonia-specific Escherichia coli with distinct phylogenetic and virulence profiles, France, 2012-2014. Emerg. Infect. Dis. *25*, 710–718. https://doi.org/10.3201/eid2504.180944.

Leitner, L., Ujmajuridze, A., Chanishvili, N., Goderdzishvili, M., Chkonia, I., Rigvava, S., Chkhotua, A., Changashvili, G., McCallin, S., Schneider, M.P., et al. (2020). Intravesical bacteriophages for treating urinary tract infections in patients undergoing transurethral resection of the prostate: a randomised, placebo-controlled, double-blind clinical trial. Lancet Infect. Dis. *21*, 427–436. https://doi.org/10.1016/S1473-3099(20)30330-3.

Leung, C.Y.J., and Weitz, J.S. (2017). Modeling the synergistic elimination of bacteria by phage and the innate immune system. J. Theor. Biol. *429*, 241–252. https://doi.org/10.1016/j.jtbi.2017.06.037.

Levin, B.R., Baquero, F., Ankomah, P.P., and McCall, I.C. (2017). Phagocytes, antibiotics, and self-limiting bacterial infections. Trends Microbiol. *25*, 878–892. https://doi.org/10.1016/j.tim.2017.07.005.

Lin, Y., Quan, D., Yoon Kyung Chang, R., Chow, M.Y.T., Wang, Y., Li, M., Morales, S., Britton, W.J., Kutter, E., Li, J., and Chan, H.K. (2020). Synergistic

activity of phage PEV20-ciprofloxacin combination powder formulation-A proof-of-principle study in a P. aeruginosa lung infection model. Eur. J. Pharm. Biopharm. *158*, 166–171. https://doi.org/10.1016/j.ejpb.2020.11.019.

Lourenco, M., Chaffringeon, L., Lamy-Besnier, Q., Pedron, T., Campagne, P., Eberl, C., Berard, M., Stecher, B., Debarbieux, L., and De Sordi, L. (2020). The spatial heterogeneity of the gut limits predation and fosters coexistence of bacteria and bacteriophages. Cell Host Microbe *28*, 390–401.e5. https://doi.org/10.1016/j.chom.2020.06.002.

Luong, T., Salabarria, A.C., and Roach, D.R. (2020). Phage therapy in the resistance era: where do we stand and where are we going? Clin. Ther. *42*, 1659–1680. https://doi.org/10.1016/j.clinthera.2020.07.014.

Marriott, H.M., and Dockrell, D.H. (2007). The role of the macrophage in lung disease mediated by bacteria. Exp. Lung Res. *33*, 493–505. https://doi.org/10.1080/01902140701756562.

Marshall, S., Madabushi, R., Manolis, E., Krudys, K., Staab, A., Dykstra, K., and Visser, S.A.G. (2019). Model-informed drug discovery and development: current industry good practice and regulatory expectations and future perspectives. CPT Pharmacometrics Syst. Pharmacol. *8*, 87–96. https://doi.org/10.1002/psp4.12372.

Melo, L.D.R., Oliveira, H., Pires, D.P., Dabrowska, K., and Azeredo, J. (2020). Phage therapy efficacy: a review of the last 10 years of preclinical studies. Crit. Rev. Microbiol. *46*, 78–99. https://doi.org/10.1080/1040841x.2020.1729695.

Messika, J., Magdoud, F., Clermont, O., Margetis, D., Gaudry, S., Roux, D., Branger, C., Dreyfuss, D., Denamur, E., and Ricard, J.D. (2012). Pathophysiology of Escherichia coli ventilator-associated pneumonia: implication of highly virulent extraintestinal pathogenic strains. Intensive Care Med. *38*, 2007–2016. https://doi.org/10.1007/s00134-012-2699-5.

Morello, E., Saussereau, E., Maura, D., Huerre, M., Touqui, L., and Debarbieux, L. (2011). Pulmonary bacteriophage therapy on Pseudomonas aeruginosa cystic fibrosis strains: first steps towards treatment and prevention. PLoS One *6*, e16963. https://doi.org/10.1371/journal.pone.0016963.

Morin, C.E., and Kaper, J.B. (2009). Use of stabilized luciferase-expressing plasmids to examine in vivo-induced promoters in the Vibrio cholerae vaccine strain CVD 103-HgR. FEMS Immunol. Med. Microbiol. *57*, 69–79. https://doi.org/10.1111/j.1574-695x.2009.00580.x.

Oechslin, F., Piccardi, P., Mancini, S., Gabard, J., Moreillon, P., Entenza, J.M., Resch, G., and Que, Y.A. (2017). Synergistic interaction between phage therapy and antibiotics clears Pseudomonas aeruginosa infection in endocarditis and reduces virulence. J. Infect. Dis. *215*, 703–712. https://doi.org/10.1093/infdis/jiw632.

Payne, R.J., and Jansen, V.A. (2001). Understanding bacteriophage therapy as a density-dependent kinetic process. J. Theor. Biol. *208*, 37–48. https://doi.org/10.1006/jtbi.2000.2198.

Payne, R.J., and Jansen, V.A. (2003). Pharmacokinetic principles of bacteriophage therapy. Clin. Pharmacokinet. *42*, 315–325. https://doi.org/10.2165/00003088-200342040-00002.

Perelson, A.S., and Guedj, J. (2015). Modelling hepatitis C therapy–predicting effects of treatment. Nat. Rev. Gastroenterol. Hepatol. *12*, 437–445. https://doi.org/10.1038/nrgastro.2015.97.

Pouillot, F., Chomton, M., Blois, H., Courroux, C., Noelig, J., Bidet, P., Bingen, E., and Bonacorsi, S. (2012). Efficacy of bacteriophage therapy in experimental sepsis and meningitis caused by a clone O25b:H4-ST131 Escherichia coli strain producing CTX-M-15. Antimicrob. Agents Chemother. *56*, 3568–3575. https://doi.org/10.1128/aac.06330-11.

Roach, D.R., Leung, C.Y., Henry, M., Morello, E., Singh, D., Di Santo, J.P., Weitz, J.S., and Debarbieux, L. (2017). Synergy between the host immune system and bacteriophage is essential for successful phage therapy against an acute respiratory pathogen. Cell Host Microbe *22*, 38–47.e4. https://doi.org/10.1016/j.chom.2017.06.018.

Sarker, S.A., Sultana, S., Reuteler, G., Moine, D., Descombes, P., Charton, F., Bourdin, G., McCallin, S., Ngom-Bru, C., Neville, T., et al. (2016). Oral phage therapy of acute bacterial diarrhea with two coliphage preparations: a randomized trial in children from Bangladesh. EBioMedicine *4*, 124–137. https://doi.org/10.1016/j.ebiom.2015.12.023.

Schooley, R.T., Biswas, B., Gill, J.J., Hernandez-Morales, A., Lancaster, J., Lessor, L., Barr, J.J., Reed, S.L., Rohwer, F., Benler, S., et al. (2017). Development and use of personalized bacteriophage-based therapeutic cocktails to treat a patient with a disseminated resistant acinetobacter baumannii infection. Antimicrob. Agents Chemother. *61*, e00954-17. https://doi.org/10.1128/aac.00954-17.

Smith, A.M., McCullers, J.A., and Adler, F.R. (2011). Mathematical model of a three-stage innate immune response to a pneumococcal lung infection. J. Theor. Biol. *276*, 106–116. https://doi.org/10.1016/j.jtbi.2011.01.052.

Smith, H.W., Huggins, M.B., and Shaw, K.M. (1987). The control of experimental Escherichia coli diarrhoea in calves by means of bacteriophages. J. Gen. Microbiol. *133*, 1111–1126. https://doi.org/10.1099/00221287-133-5-1111.

Sousa, J.A.M.D., and Rocha, E.P.C. (2019). Environmental structure drives resistance to phages and antibiotics during phage therapy and to invading lysogens during colonisation. Sci. Rep. *9*, 3149. https://doi.org/10.1038/s41598-019-39773-3.

Weld, R.J., Butts, C., and Heinemann, J.A. (2004). Models of phage growth and their applicability to phage therapy. J. Theor. Biol. *227*, 1–11. https://doi.org/10.1016/s0022-5193(03)00262-5.

STAR★METHODS

KEY RESOURCES TABLE

REAGENT or RESOURCE	SOURCE	IDENTIFIER
Bacterial and virus strains		
Escherichia coli 536-lux	Dufour et al. (2015)	N/A
Bacteriophage 536_P1	Dufour et al. (2015)	N/A
Experimental models: Organisms/strains		
Mouse Balb/cJRj	Janvier Labs	N/A
Software and algorithms		
Prism	GraphPad	Version 8
Monolix (algorithm SAEM)	Lixoft	Version 2018R2
R	The R foundation	Version 3.4.3.

RESOURCE AVAILABILITY

Lead contact

Further information and requests for resources, reagents and numerical codes should be directed to and will be fulfilled by the lead contact, Laurent Debarbieux (laurent.debarbieux@pasteur.fr).

Materials availability

The bacterial strain 536-lux and the phage 536_P1 are available from the lead contact upon completion of a Materials Transfer Agreement (MTA).

Data and code availability

- Data is available from the lead contact upon request.
- The original code of the phage-bacteria mathematical model is available as Data S1 in the supplemental information and software used are reported in the key resources table.
- Any additional information required to reanalyze the data reported in this paper is available from the lead contact upon request.

EXPERIMENTAL MODELS AND SUBJECT DETAILS

Ethic statement

A total of 241 eight-week-old BALB/cJRj male mice (Janvier Labs, France) were housed in animal facility in accordance with French and European regulations on the care and protection of laboratory animals. Food and drink were provided ad libitum. Protocol was approved by the veterinary staff of the Institut Pasteur animal facility (approval number 20.173) and the National Ethics Committee regulating animal experimentation (APAFIS#26874-2020081309052574 v1).

Phages and bacterial strains

The *E coli* strain 536 and phage 536_P1 were previously described as reported in the key resources table.

METHOD DETAILS

Purification of bacteriophages

Phage 536_P1 was amplified on strain 536 and purified by first, filtration of lysate to 0.1 μm followed by tangential ultrafiltration (Vivaflow™, Sartorius, 100 kDa), two ultracentrifugations on cesium chloride, dialysed against TN (Tris-HCl pH8, NaCl 150 mM), passed three times through an endotoxin removal column (Endotrap Blue, Hyglos, Germany) and filtered-sterilized at 0.22 μm.

Determination of *in vitro* infection parameters of phage 536_P1

Parameters of the interactions between strain 536 and phage 536_P1 have been determined *in vitro*, notably the rate of transition *e* from infected non-productive bacteria to productively infected bacteria (eg, log(2)/e is the median eclipse phase duration), and the burst size *b*, *i.e.* the number of virions released by a lysed bacteria. The median eclipse phase time and the burst size were estimated

from non-linear mixed effect models performed with the SAEM algorithm implemented in Monolix software (version 2018R2) (Kuhn and Lavielle, 2005) using data from one-step-growth experiments (see Supplemental information).

One-step-growth experiments

The one-step growth experiment was performed in triplicate, using Luria Bertani Broth (Lennox). As previously described (Hyman and Abedon, 2009), an exponential-phase culture (9 mL) of strain 536 (optical density at 600 nm 0.25, *ie* 9 $\log_{10}$ CFU) was mixed with 1 mL of 8 $\log_{10}$ PFU of phage 536_P1 (MOI of 0.1). The mixture was placed under constant shaking (100 rpm) at 37°C. Duplicated samples were collected at 2-min intervals during 30 min. Six minutes after mixing phages and bacteria, the mixture was 1000 fold diluted in LB medium in order to lower bacterial concentration and avoid any reinfection. Out of the duplicated samples, one was immediately diluted and plated for phage titration, while the second was treated with 10% (vol/vol) chloroform to release intracellular phages in order to determine the eclipse period before phage titration.

Dynamic quantification of bacteria and phages over time

We first established the correlation between optical density and CFU for strain 536 by plating on LB agar dilutions of independent aliquots of exponentially growing cells from which OD600 nm was recorded before dilutions. Then, an exponential bacterial culture (50 mL of a total of 8.7 $\log_{10}$ CFU) was mixed with 5.7 $\log_{10}$ PFU (ie MOI 1×10^{-3}) and incubated under constant shaking (150 rpm, 37°C). Samples from this mixture were withdrawn at specific time points to measure optical density at 600 nm and count the number of phages after serial dilutions and plating on LB agar covered with strain 536. Experiments were performed three times from independent cultures.

Kinetic of lysis

To assess the behavior of strain 536 in presence of phage 536_P1 at different MOI, OD600 nm was recorded over time from microtiter plates. In each well, 180 μL of an exponential culture of strain 536 (OD 0.1) was mixed with 20 μL of phage 536_P1 at different concentrations (each replicated six times) to reach MOI of 0.001; 0.01; 0.1; 1 and 10. Controls included wells with phage alone, or bacteria alone or LB alone. The microplates were incubated in a microplate reader (Tecan) set at 37°C during 12 h with orbital agitation. Three independent experiments were performed.

In vitro data analysis

Models of *in vitro* data were built using similar methodology used for analyzing *in vivo* PK/PD data: parameters of mixed models were estimated using SAEM algorithm and the model selection was based on BIC. Model of phage/bacteria interactions *in vitro* was built in three steps.

First, one step growth experiments reproduced a single lysis cycle of the phage and therefore allowed to estimate the burst size (*i.e.* the number of virions relased from each bacterium lysed) and the time of a cycle, including an eclipse period. The best fit of these one step growth data was obtained using a multiple transit compartments model. The burst size (570 virions/CFU) was estimated with acceptable precision of estimation (relative standard error < 30%). To confirm this burst size value which was higher than expected, another estimation method was used. A nonlinear regression was performed ($y(t) = E0 + \frac{Emax}{1+10^{(T50-t)\gamma}}$, with $y(t)$ in $\log_{10}$ PFU/infected cell, $E0$ the baseline, $Emax$ the plateau, $log(T50)$ the time to reach $\frac{E0+Emax}{2}$ and γ a shape parameter) on the mean data from the three different experiments. A burst size $\left(b = \frac{10^{Emax} - 10^{E0}}{10^{E0}}\right)$ of 554 virions/CFU was estimated from the estimates of this nonlinear regression, which was close to the value obtained from the nonlinear mixed effect model. The median period for a phage to produce and release new phages was estimated at 35 min. Second, bacterial growth was characterized from the above *in vitro* experiments exploiting the condition MOI 0 (without any phage). The bacterial doubling time was estimated at 63 min from the model. Third, lysis kinetics experiments (at MOI> 0) were modelled using a predator-prey model with similar structure to *in vivo* model (see equations below and Table S1). The burst size and bacterial growth were fixed at values respectively obtained at the above first and second steps. The lysis rate (corresponding to rate between infected latent and infected productive bacteria) was fixed from one step growth experiments on 536_P1. The eclipse period was obtained by sensitivity analysis on the transition rate e. The proportion of phage-resistant clones at baseline and their relative fitness (w) were characterized from this model.

$$\frac{dS}{dt} = \alpha\left(1 - \frac{S + I_1 + I_2 + R}{10^{B_{max}}}\right)S - \beta VS$$

$$\frac{dI_1}{dt} = \beta VS - eI_1$$

$$\frac{dI_2}{dt} = eI_1 - \delta_V I_2$$

$$\frac{dR}{dt} = w\alpha\left(1 - \frac{S + I_1 + I_2 + R}{10^{B_{max}}}\right)R$$

$$\frac{dV}{dt} = -\beta VS + \delta_V b I_2$$

Presentation of the murine model of pulmonary phage therapy

The *E. coli* strain 536 is a virulent clinical strain belonging to the B2 phylogenetic group (Brzuszkiewicz et al., 2006). The *E. coli* strain 536-lux was obtained by the transformation of wild-type 536 strain with plasmid pCM17, which carries the *luxCDABE* operon from *Photorhabdus luminescens* under *OmpC* promoter (Morin and Kaper, 2009). This plasmid is stable over 7 days without adding antibiotic in the medium (Dufour et al., 2015).

Phage 536_P1 (Dufour et al., 2015) is a virulent *Myoviridae* (149.4 Kb) that was amplified on strain 536 and purified according to molecular biology protocols including an endotoxin removal step (Endotrap Blue, Hyglos, Germany). The stock solution of 8.2 $\log_{10}$ PFU/mL has an endotoxin concentration of 2.15 EU/mL.

Pneumonia was induced by intratracheal (IT) administration of strain 536-lux in eight-week-old BALB/cJRj anesthetized male mice (mixture of Ketamine and Xylazine administered intraperitoneally, IP). IT was performed using elongated tips guided by the glottis visualization with a cold light. The correct position of the tip was checked by the liquid movement inside the tip caused by the ventilatory movement of the animal. The liquid was then expulsed from the tip with a pipette, and 100 μL of air was then pushed to aerosolize the solution to the lower airways. Mice were maintained in prone position during at least 5 min. Exponentially growing bacteria in Luria Bertani Broth (Lennox) at 37°C were centrifuged and washed twice and finally resuspended in PBS to obtain inoculums ranging from 7.6 to 8.2 $\log_{10}$ CFU in 20μL. Previous work showed that a single intranasal dose of 7.6 $\log_{10}$ CFU led to a fatal outcome at 72 h post-infection for 100% of mice. Moreover, mice similarly infected were successfully treated (100% survival 10 days post-infection) when a single intranasal dose of 7.0 $\log_{10}$ PFU of phage 536_P1 was administered 2 h post-infection (Dufour et al., 2015).

Phage treatment was applied under general anesthesia (isoflurane, inspired fraction = 2%) using IT or intravenous (IV, retro-orbital injection) administration two hours after infection. A volume of 20μL of phage 536_P1 was used, containing either a low (Lo; 6.6 $\log_{10}$ PFU), medium (Me; 7.6 $\log_{10}$ PFU) or high (Hi; 8.6 $\log_{10}$ PFU) amount of phages.

At 2, 4, 8, 24 and 48 h after phage administration, mice were sacrificed, and blood (in heparin coated tubes) and lungs were recovered and put on ice. Lungs were weighted, homogenized in PBS with protease inhibitor (EDTA free micro Tabs, SigmaAldrich). Lungs and blood were then centrifuged (5000 g, 15 min, 4°C). The supernatant was collected, serially diluted and spotted (in triplicate) on agar plates covered with strain 536 to titer phage 536_P1.

Bioluminescence and longitudinal follow up of bacterial load in lungs

In all our experiments photon emission of the luminescent bacteria was recorded at regular intervals under general anesthesia (isoflurane, inspired fraction = 2%) using IVIS Spectrum and analyzed with Living Image software (PerkinElmer, Richmond, CA) as previously described (Debarbieux et al., 2010). Photons emitted within the chest area of each mouse were collected as photon/s/cm^2/steradian.

To fully exploit the *in vivo* imaging tool we established the correlation between bioluminescence and CFU count in lungs using data from 17 untreated animals that were euthanized at different time points and for which lung bacteria was quantified by plating (Figure S1). The relationship obtained allowed us to derive from the luminescence signal an equivalent counts of CFU per gram of lung (noted CFUeq/g) that was used to obtain in all infected animals (untreated or treated by phages) the bacterial densities. The accuracy of this correlation curve was tested against previously published mice lungs CFUs data obtained 6 h post-infection by the bioluminescent strain 536 (Dufour et al., 2015). The corresponding amount of emitted light was retrieved for 8 animals and was converted to obtain CFUeq/g. The median predicted value was 2.3×10^7 CFUeq/g (interquartile range: [1.9×10^7, 3.2×10^7]), which is close to the observed value of 8.3×10^6 CFU/g (interquartile range: [5.2×10^6, 1.0×10^7]) initially reported in the Table 1 of that study.

Phage distribution

A dose of 8 $\log_{10}$ PFU of phage 536_P1 was administered in uninfected mice (N = 53) using IT (N = 16) or IV (N = 37) route. At 2, 4, 8, 24 and 48 h after phage administration, mice were sacrificed, and blood (in heparin coated tubes) and lungs were recovered and put on ice. Lungs were weighted, homogenized in PBS with protease inhibitor (EDTA free micro Tabs, SigmaAldrich). Lungs and blood were then centrifuged (5000 g, 15 min, 4°C). The supernatant was collected, serially diluted and spotted (in triplicate) on agar plates covered with strain 536 to titer phage 536_P1.

We used the following standard pharmacokinetic model to estimate phage biodistribution:

$$\frac{dV_B}{dt} = -k_a V_B \qquad \text{(Equation 1)}$$

$$\frac{dV}{dt} = Fk_aV_B - k_eV \quad \text{(Equation 2)}$$

where V and V_B denote phage quantity in lung and blood compartments, respectively, k_e is the elimination rate from lungs, k_a is the transfer rate from blood to lungs, F is the bioavailability in lungs after IV administration. The initial condition of these equations are $V_B(0) = dose$ and $V(0) = 0$ in case of IV administration and $V_B(0) = 0$ and $V(0) = dose$ in case of IT administration. V is divided by the phage distribution weight (W) to obtain the phage concentration in lung compartment. Before the modeling analysis, the median phage concentration at baseline (8 $\log_{10}$ PFU/g) was determined following the IT administration of a single dose of 8 $\log_{10}$ PFU, and F was obtained by performing the ratio of IV/IT area under the curves in the lungs. The parameter W was deduced from the phage concentration at baseline. Estimations of the other parameters were performed by naive pooling of data (i.e. considering all the measures for each group (IV and IT) as if they came from a single individual and performing a nonlinear regression).

Bacterial kinetics in untreated mice

We characterize the natural bacterial kinetics (i.e., in absence of treatment) in animals infected with doses of 7.6 $\log_{10}$ CFU (34 mice) or 8.2 $\log_{10}$ CFU (12 mice) and the bacterial kinetics obtained by bioluminescence (see above) using the following model (one mouse was not analyzed due to death during bacterial inoculation, i.e. N = 45):

$$\frac{dB}{dt} = \alpha\left(1 - \frac{B}{B_{max}}\right)B - \delta_M\frac{B}{B_{50}+B} \quad \text{(Equation 3)}$$

Where α is the exponential growth rate of bacteria (eg, log(2)/α is the doubling time) and B_{max} is the maximal carrying capacity, determined by sensitivity analysis. The initial condition of B was estimated by the parameter B_0 ($B(0) = 10^{B_0}$). Consistent with previous work (Dufour et al., 2019), we assumed that in the first 3 h of infection the immune system had no activity (eg, bacteria could grow exponentially during this period). After this period the elimination of bacteria by the host was modeled by a non-linear saturable term, given by $\delta_M\frac{S}{B_{50}+B}$.

Phage-bacteria interaction in treated mice

We characterized phage-bacterial interactions using data obtained in 142 mice infected by 7.6 $\log_{10}$ CFU and treated subsequently (four mice were not analyzed due to death during bacterial inoculation, i.e. N = 138), using the protocol described above, with a single dose (low, medium or high) of phages administered using IT or IV route (detail of the groups in Figure 1). Bacterial kinetics was derived from bioluminescence (see above) and lungs were collected at 2, 4, 8, 24 or 48 h after phage administration to count PFU. We also considered data in untreated mice (see previous section) for the analysis.

A linear mixed model of longitudinal bacterial load has been built using the lmer function of the lme4 R package lmer. Two covariates were considered: the treatment (untreated or treated) and the inoculum (<6.8 $\log_{10}$ CFUeq/g) or ($\geq$6.8 $\log_{10}$ CFUeq/g). The basis model included the intercept, the slope (time effect), the treatment and the inoculum effect on the intercept, the inoculum effect on the slope and the interaction between the inoculum and the treatment. The final model included these parameters as well as the treatment effect on the slope. To evaluate the phage treatment effect on the bacterial load evolution, a likelihood ratio test was performed to compare the two nested model.

The model describing interactions between phage 536_P1 and strain 536 relied on a system of ordinary differential equations (ODE) (Figure 1, Equations 4, 5, 6, 7, 8, 9, and 10, presented below). We combined standard model of viral (Perelson and Guedj, 2015) and bacterial kinetics (Friberg and Guedj, 2020) to tease out the main parameters governing phage-bacteria interaction in mice. In lungs, phages can infect susceptible bacteria (S) following a mass-action term, with rate β. We also considered a population of refractory bacteria (of initial proportion f), noted R, that includes both phage-resistant and phage-inaccessible bacteria.

$$\frac{dS}{dt} = \alpha\left(1 - \frac{S+I_1+I_2+R}{B_{max}}\right)S - \delta_M\frac{S}{B_{50}+S+I_1+I_2+R} - \beta VS \quad \text{(Equation 4)}$$

$$\frac{dI_1}{dt} = \beta VS - eI_1 - \delta_M\frac{I_1}{B_{50}+S+I_1+I_2+R} \quad \text{(Equation 5)}$$

$$\frac{dI_2}{dt} = eI_1 - \delta_V I_2 - \delta_M\frac{I_2}{B_{50}+S+I_1+I_2+R} \quad \text{(Equation 6)}$$

$$\frac{dR}{dt} = \alpha\left(1 - \frac{S+I_1+I_2+R}{B_{max}}\right)R - \delta_M\frac{R}{B_{50}+S+I_1+I_2+R} \quad \text{(Equation 7)}$$

$$\frac{dV_B}{dt} = -k_a V_B \quad \text{(Equation 8)}$$

$$\frac{dV}{dt} = -\beta VS + b\delta_V I_2 + Fk_a V_B - k_e V \quad \text{(Equation 9)}$$

We considered the following initial condition for this system: $S(0) = 10^{B_0}(1-f), I_1(0) = 0, I_2(0) = 0, R(0) = 10^{B_0} \times f, V_B(0) = 0, V(0) = 0$. The dose of phages is added to V or V_B at the phage administration time by IT or IV route, respectively.

Non-linear mixed effect model for phage-bacteria interactions

The model parameters in bold were estimated using data from all infected animals while all other parameters were fixed to the values determined above, either *in vitro* (e, b), in uninfected treated mice (k_a, F, k_e) or in infected untreated mice ($\alpha, B_{max}, \delta_M, B_{50}$). All inference procedures were performed in a non-linear mixed effect model framework using the SAEM algorithm implemented in Monolix software (Kuhn and Lavielle, 2005) (see the phage-bacteria mathematical model reported in Data S1 and related to Figure 5). All inference procedures assumed an additive Gaussian error model on the log-transformed data, with σ_B (resp. σ_V) representing the standard deviation of the measurement error associated with bacterial load (resp. phage concentration). All parameters along with their estimated standard error are summarized in Table 1.

Impact of bacterial kinetics on survival

Finally, we aimed to consider the potential bias due to the fact that more severely infected animals died earlier, making the population study less and less representative as time goes by. In this approach, called joint models (Desmee et al., 2015), the probability to survive up to time t, $S(t)$, is modeled as: $S(t) = e^{-\int_0^t h(t)dt}$ where

$$h(t) = \frac{\kappa}{\lambda}\left(\frac{t}{\lambda}\right)^{\kappa-1} e^{\gamma \times log(S(t)+I_1(t)+I_2(t)+R(t))} \quad \text{(Equation 10)}$$

h(t) is the instantaneous hazard function, κ and λ are scale parameters characterizing the risk of death in absence of infection and γ quantifies the impact of bacterial load on mortality. Thus, in this model $\gamma = 0$ is indicative of an absence of association between bacterial load and mortality, while $\gamma > 0$ indicates that increased bacterial load is associated with an increased risk of death.

Model evaluation

Individual fits were investigated to evaluate the different models. For the final model, we also evaluated the model predictions i) for the bacterial kinetics by using prediction corrected-visual predictive checks (Bergstrand et al., 2011), accounting for the risk of death and ii) visual predictive checks of the survival. Simulations for validation methods were made using mlxR package.

Model based simulations for the impact of treatment procedures and phage parameter values

Model based predictions were performed to investigate various scenarios as follows. For each simulation, the median profile of different model compartments (S, R, I_1, I_2 and V) was investigated using the parameters determined in Table 1 and different experimental conditions regarding the route of administration (IV or IT), the dose of phage administered (Lo: 5.6, Med: 7.6 or Hi: 8.6 $\log_{10}$ PFU) and initial bacterial load (6, 7 or 8 $\log_{10}$ CFUeq/g). We also evaluated the effects of different burst size (10 fold lower, 10 fold larger than the estimated value *in vitro*), using a single initial bacterial load of 7 $\log_{10}$ CFUeq/g. Furthermore, when setting a burst size 10 times lower than the estimated value (and a fixed initial bacterial load of 7 $\log_{10}$ CFUeq/g), we investigated the effect of three different lysis rates values: the value estimated *in vivo* (0.09 h^{-1}); a value three times higher (0.27 h^{-1}); a value estimated *in vitro* (1.39 h^{-1}).

QUANTIFICATION AND STATISTICAL ANALYSIS

Quantification and statistical analysis reported in this work are described in the corresponding Method details sections or figure legends. The statistical procedures were performed using R, except for those related to non-linear mixed effects models which were performed with Monolix.